Comparative studies about CO methanation over Ni(211) and Zr-modified Ni(211) surfaces: Qualitative insight into the effect of surface structure and composition

Cuimei Zhi [a,b], Riguang Zhang [a], Baojun Wang [a,*]

[a] Key Laboratory of Coal Science and Technology of Ministry of Education and Shanxi Province, Taiyuan University of Technology, Taiyuan 030024, China
[b] College of Chemistry and bioengineering, Taiyuan University of Science and Technology, Taiyuan 030021, China

ABSTRACT

In order to reveal the underlying mechanism of coke-deposition resistance of the promoter Zr, the comparative studies about the reaction pathways of CO methanation have been carried out over the stepped Ni(211) and Zr-modified Ni(211) surfaces using the density functional theory. DFT results show that $CO \rightarrow COH \rightarrow \textbf{C} \rightarrow CH \rightarrow CH_2 \rightarrow CH_3 \rightarrow CH_4$ and $CO \rightarrow COH \rightarrow HCOH \rightarrow CH_2OH \rightarrow CH_2 \rightarrow CH_3 \rightarrow CH_4$ are mainly responsible for CH_4 formation on Ni(211). Thus, in the former pathway, the main contributor to carbon deposition is the dissociation of COH; while in the latter pathway, carbon formation ascribes to the decomposition of CH_2 due to the competition of CH_2 between hydrogenation and dehydrogenation. Conclusively, Ni(211) is much susceptible to carbon formation. However, ZrNi(211) surface exhibits high resistance to carbons with the energetically favorable pathway of $CO \rightarrow HCO \rightarrow CH_2O \rightarrow CH_2OH \rightarrow CH_2 \rightarrow CH_3 \rightarrow CH_4$ since CH_2 prefers to be hydrogenated to CH_3 rather than being dehydrogenated into CH. On the other hand, for the effects of surface structure and composition on the selectivity, Ni(211) displays a remarkable increase in selectivity to CH_4 compared to Ni(111), which ascribes to much difference in the activity of CH_2OH between the dissociation to CH_2 and the hydrogenation to CH_3OH, the former is superior to the latter. On ZrNi(211), even no CH_3OH yield is expected. Further, the presence of promoter Zr greatly decreases the overall activation energy of CH_4 formation on ZrNi(211) surface, this results in a significant increase of the reaction activity compared to Ni(111) and Ni(211). To sum up, ZrNi(211) is highly activity and selectivity of CH_4 formation in CO methanation, and particularly resistant to carbon formation, which will provide a way of fabricating a more effective Ni-based catalyst.

1. Introduction

CO methanation has received broad attention in practical applications [1–5]. Ni-based catalysts have been widely used for this process. However, since CO methanation is highly exothermic, the catalytic performance of pure Ni catalyst would gradually decrease and even deactivate due to the severe carbon deposition. The concerns over Ni deactivation via carbon formation motivate interest in new catalysts to inhibit carbon formation and keep the activity of CO methanation, which become one of the major challenges to develop a more effective Ni-based catalyst in CO methanation.

Four different mechanisms: (a) CO direct dissociation, (b) CO disproportionation, (c) COH dissociation, and (d) thermal decomposition of $CH_x(x = 1\text{-}3)$, have been identified for the origination of carbon formation, in which CH_x species is formed by the C—O bond cleavage of the hydrogenated intermediates $CH_xO(H)(x = 1\text{-}3)$ during methanation, and as the major intermediate is detected on Ni surface in the earlier studies [6]. Previous studies showed that the former two reactions as carbon sources are unlikely on the defect-rich Ni surface, and the C—O bond is only breakable at the step and defect sites via H-assisted route [7]; carbon formation is derived from the latter two reactions.

This is indeed shown to be the case in some other reports, it has been demonstrated that the dissociation of COH at the step site is the rate-limiting step (RLS), and it is assigned as the evidence of carbon formation under the appropriate methanation conditions [6,8]. This is also supported by the earlier conclusion of Coenen et al., who claimed that the hydrogenation of CH_x, for instance, CH_2 intermediate, is assumed to the RLS in the methanation process [9,10]. This means that, COH dissociation and CH_x decomposition are the main

contributors to carbon species, and one effective way to prevent carbon deposition is to promote CH_x hydrogenation to CH_4 and suppress CH_x dehydrogenation to C accordingly. Thus, decreasing the rate of COH dissociation and decrease/avoid the formation of COH is another approach to improve the carbon resistance of Ni catalyst.

In general, the flat Ni(111) is less prone for the accumulation of C centers, irrespective of its origin, in comparison to the situation on steps, as less active for C centers formation [11]. previous studies [12] found that the dominate existence form of CH_x is CH, formed by the pathway of CO → HCO (or HCO → HCOH) → CH on the terrace Ni(111) surface; and it is noteworthy that, CH prefers to be hydrogenated to CH_2 rather than being dissociated into C, and thereby that the Ni terrace is less sensitive to carbon formation but instead of the Ni step.

Meanwhile, the Ni step atoms play important roles as the active sites for CO methanation, as the highly structure sensitive [3,6,8], the steps are the only relevant sites to dissociate CO, and with no steps, CO methanation reaction would come to a halt, and less carbon is deposited [13]. Therefore, the Ni step is more likely to be covered and blocked by carbon species, leading to deactivate the catalyst during CO methanation. This suggests that carbon deposits ascribed to CH_x decomposition and/or COH dissociation, which is closely related to the Ni step sites, and in reality, the most common step sites for Ni catalyst exist on the defect Ni(211) surface.

It is therefore, confirming the main existence form of CH_x species on the stepped Ni(211) surface should be carried out by the studies about the reaction routes of CH_4 formation. Afterwards, improving CH_x hydrogenation and suppressing its dehydrogenation are of vital importance to resistance of carbon formation. Thus, $CH_xO(H)$ plays an active role: the relative activity of $CH_xO(H)$ dissociation and hydrogenation is predicted to be one of the key factor, which controls the selectivity to CH_4. Accordingly, facilitating the C—O bond breakage of the hydrogenated intermediates $CH_xO(H)$ as far as possible and reducing $CH_xO(H)$ hydrogenation to the byproduct CH_3OH are beneficial to an enhancement of CH_4 productivity. In response to the two purposes, one approach is connected with the modification of Ni structure by the formation of Ni-based alloys with adding promoters.

Several combinations, such as Fe/Ni [14], Zr/Ni [1–5,15–17], V/Ni [18], and Ti/Ni [19], have been experimentally proved to be an effective to suppress carbon deposition and improve CH_4 productivity simultaneously. Theoretically, it has been reported that Fe/Ni [14] alloy leads to a remarkable increase of the activity of CO methanation due to the lower activation energy of the rate-limiting step comparative to the pure Ni catalyst, and CH is identified as the dominant CH_x, associated with the C—O bond cleavage HCO, followed by the sequential hydrogenations to eventually CH_4. In addition, Fajín et al. [20] pointed out that both Ru/Ni and Rh/Ni alloys can lead to an increase in selectivity of CH_4 in contrast with the pure Ni catalyst, moreover, the stepped Ni(211) shows a high selective toward CH_4 compared to the flat Ni(111).

Notably, Zr/Ni alloy exhibits high CO conversion and CH_4 selectivity as well as superior resistant to carbon formation in a broad temperature range of 300 ∼ 550 °C [1–5,15–17]. This is caused by the formation of nickel zirconium solid solution, which produces sufficient Ni particles with appropriate size and dispersion and ensures the more active sites for the catalytic processes, comparative to the free Ni species, which are poorly dispersed and possess less available active sites. This implies that the added Zr plays a positive role in improving Ni catalytic performance. However, the principal reason of the observed distinctive properties by introducing Zr additive is still unclear.

Insight into the underlying mechanism of CO methanation on the stepped and Zr-modified Ni(211) surface, and simultaneously probing into the role of Zr promoter, may shed light on some key issues: (1) What is the most favorable pathway of CO methanation on both surfaces? (2) What is the key step to control CH_4 productivity? (3) What is the most favored CH_x monomer? Whether CH_x dissociation causes carbon formation or not? (4) How does the stepped surface affects the selectivity of CH_4 compared to the flat Ni(111) surface? (5) How does the Zr-modified stepped Ni(211) surface improves the activity of CO methanation and increases the selectivity to CH_4 as well as restrains carbon formation compared to the pure Ni(211) surface?

In attempting to tackle above these puzzles, in this study, DFT calculations have been carried out to compare and illustrate the promoted behavior of the modified catalyst in catalytic performance as well as the resistance to carbons. This study is organized as follows: the computational details are outlined in Section 2. The results including the structures and energies of the related species, as well as the activation energy and reaction energy of all elementary steps, are identified in Section 3, herein, the effects of Zr promoter and the stepped surface on the activity and selectivity of CO methanation, related to CH_4, CH_3OH and carbon formation, have been discussed. The conclusion is summarized in Section 4.

2. Computational details

2.1. Calculated models

The stepped Ni(211) surface with the terrace sites and under-coordinated step sites is employed to model the Ni catalyst with surface defects, as shown in Fig. 1(a), an eight-layer slab with a $p(2 \times 3)$ supercell is used, the uppermost five layers together with the adsorbed species are fully relaxed, and the bottom three layers are fixed at their bulk positions. The slab is separated by 15 Å vacuum to ensure the negligible interaction between the adsorbates and the slab. Nine possible adsorption sites exist on the stepped Ni(211) surfaces: the Se-top, Se-bridge, Se-fcc, and Se-hcp sites at the step, the Le-top, Le-bridge, Le-fcc, and Le-hcp sites at the terrace, and the 4-hollow site.

Previous studies have confirmed that the strong Zr—Ni bond, resulting from the s-d and d-d hybridizations, can be formed at Zr/Ni interface by introducing Zr into Ni; the length of Zr—Ni bond by substitution is closer to the equilibrium value of 2.63 Å [21]. Zr can selectively deposit on Ni surface of Zr-decorated Ni/γ-Al$_2$O$_3$ catalyst due to the electrostatic interaction [15], and alloying additions tend to segregate at the Ni/ZrO$_2$ interfaces due to the minimized Gibbs free energy [22]. Thus, it is reasonable that Zr promoter is only introduced into the first layer of Ni(211) surface. Further, the aim of this work is only to qualitatively reveal the role of Zr substitution at the step site in CO methanation, thereby, more than one Ni atom modification with different concentrations is not considered. The configurations with only one Zr atom replacing three Ni sites, assigned to the step, terrace and edge, are evaluated to model Zr-modified Ni(211) surface, as shown in Fig. 1(b).

The site preference of Zr substitution on Ni(211) surface is examined according to the formation energy (E_f) as follows [23].

$$E_f = E_{ZrNi(211)} + E_{Ni} - E_{Ni(211)} - E_{Zr} \quad (1)$$

Where $E_{Ni(211)}$ and $E_{Zr/Ni(211)}$ is the total energy of the Ni(211) and ZrNi(211) surfaces, respectively; E_{Ni} and E_{Zr} represent the energy of a Ni and Zr atom in bulk, respectively. A negative E_f indicates the formation of the structure is exothermic, and the more negative the E_f is, the more likely the structure is.

Based on the calculated formation energies, it is observed that Zr atom replacing the step Ni is energetic more preferable than terrace Ni. The results is further supported by the statement that the step site, possessing the significantly higher catalytic activity than the terrace and edge sites, is the predominant active center of Ni
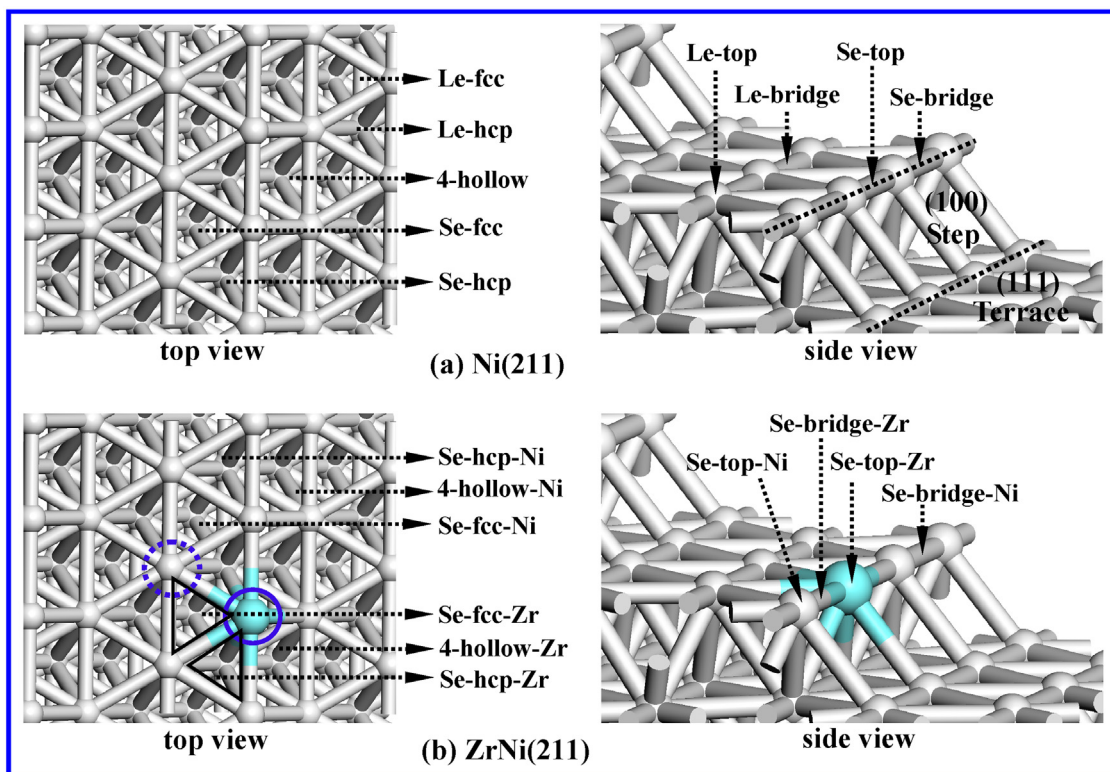
Fig. 1. Side view and top view of (a) Ni(211) and (b) ZrNi(211) surfaces.

catalyst due to the coordinatively unsaturated sites [24]. Moreover, the enormous differences in reactivity between the steps and terraces have been confirmed by DFT calculations with the ultra-high vacuum experiments [25,26]. Conclusively, Zr-modified Ni(211) surface is modeled with a Ni atom replaced by a Zr atom at the step, which is denoted as ZrNi(211) surface thought this study.

2.2. Calculated methods

DFT calculations are performed using the Vienna Ab Initio Simulation package (VASP) [27,28]. The interactions between ion cores and valence electrons are described by the projector augmented wave (PAW) method [29]. The electron exchange and correlation a treated within the generalized gradient approximation (GGA) using the Perdew-Wang 91 (PW91) functional [30,31]. Spin-polarized calculations have been considered due to the magnetic moment of Ni. The Methfessel-Paxton smearing method [32] is utilized with a width of 0.1 eV. The Brillouin zone is sampled by a $5 \times 5 \times 1$ k-point [33]. The plane-wave cutoff energy is expanded to 340 eV. The Ni lattice constant is optimized to 3.54 Å with the k points of $6 \times 6 \times 6$, which is close to the experimental values of 3.52 Å [34], and the isolated atoms and molecules in the gas phase are calculated in a $10 \times 10 \times 10$ Å cubic cell. Further, the effect of van der Waals (VDW) contributions on the adsorption of the species has been considered, in our study, the results show that all adsorbed species involved in CO methanation are chemisorption except for CH$_4$. The adsorption energies of CH$_4$ with and without DFT-D2 correction are very close on Ni(211) and ZrNi(211), as listed in Table S1, suggesting that the result of CH$_4$ physisorption obtained by the adsorption energy has not been affected by VDW calculations in our systems.

The climbing image nudged elastic band (CI-NEB) method [35,36] has been employed to study the reaction pathways. The transition state structure is deemed converged when the forces are less than 0.05 eV Å^{-1}, and the total energy difference is less than 10^{-5} eV/atom between two successive optimization processes

for the various degrees of freedom set during the calculations. The vibrational frequencies are calculated to verify the transition states with only one imaginary frequency corresponding to the desired reaction coordinates.

For the reactions on Ni(211) and ZrNi(211) surface, the activation energy (E_a) and reaction energy (ΔE) with the zero-point-energy (ZPE) corrections are defined according to the Eqs. (2) and (3) [37–39].

$$E_a = (E_{TS} - E_{IS}) + \Delta ZPE_{barrier} \tag{2}$$

$$\Delta E = (E_{FS} - E_{IS}) + \Delta ZPE_{reaction} \tag{3}$$

where E_{IS}, E_{TS} and E_{FS} correspond to the total energies of the initial states (IS), transition states (TS) and final states (FS), respectively; $\Delta ZPE_{barrier}$ and $\Delta ZPE_{reaction}$ refer to ZPE corrections for E_a and ΔE, respectively; which are determined by the Eqs. (4) and (5).

$$\Delta ZPE_{barrier} = \left(\sum_{i=1}^{vibration} \frac{h\nu_i}{2} \right)_{TS} - \left(\sum_{i=1}^{vibrations} \frac{h\nu_i}{2} \right)_{IS} \tag{4}$$

$$\Delta ZPE_{reaction} = \left(\sum_{i=1}^{vibration} \frac{h\nu_i}{2} \right)_{FS} - \left(\sum_{i=1}^{vibrations} \frac{h\nu_i}{2} \right)_{IS} \tag{5}$$

The adsorption energies (E_{ads}) are calculated by using the following Eq. (6):

$$E_{ads} = E_{s/slab} - (E_{slab} + E_s) + \Delta ZPE_{ads} \tag{6}$$

Where $E_{s/slab}$ is the total energy of the slab surface with the adsorbed species, E_{slab} is the total energy of the corresponding bare slab surface; E_s is the total energy of the gas-phase species. With this definition, the more negative E_{ads} is, the stronger the adsorption is. ΔZPE_{ads} refers to the adsorption energy with ZPE corrections. Vibrational frequencies for the species in both the gas phase and

the adsorbed state are used to determine ZPE corrections using the Eq. (7).

$$\Delta ZPE_{ads} = \left(\sum_{i=1}^{vibration} \frac{h v_i}{2} \right)_{adsorbed} - \left(\sum_{i=1}^{vibrations} \frac{h v_i}{2} \right)_{gas} \quad (7)$$

where h is Planck's constant, v_i refers to the vibrational frequencies, vibrational frequencies for the adsorbed species are determined with metal atoms fixed at their positions.

3. Results and discussion

3.1. Structures and energies of all adsorbed species

The adsorption configurations and energies of all adsorbed species involved in CO methanation are performed on Ni(211) and ZrNi(211), the most stable adsorption configurations, the corresponding adsorption energies and total charge are summarized in Fig. 2 and Table 1. To facilitate comparison, the previously published results on Ni(111) and Ni(211) available are also listed in Table 1.

3.1.1. H adsorption

Previous results [12] showed that H_2 dissociation can easily occur on Ni(111) surface due to the extremely low activation barrier (0.13 and 0.33 eV) and the strong exothermicity (1.05 and 0.77 eV) at the top and bridge sites, respectively. In this study, DFT results show that the existence form of H_2 at the Se-top site of Ni(211) is the dissociative adsorption, two dissociated H atoms is adsorbed at two adjacent Se-fcc and Se-hcp sites. H_2 dissociation at the Se-bridge site is strongly exothermic by 0.80 eV with a small activation energy of 0.14 eV. Meanwhile, H_2 dissociation at the Se-top-Zr site of ZrNi(211) is also extremely favorable with a small activation energy of 0.32 eV, and it is highly exothermic by 1.04 eV. As a result, H_2 dissociation can easily occur on Ni(211) and ZrNi(211) surfaces, which can provide the enough H atoms for CO methanation.

3.1.2. CO, COH, C, CH, CH_2, CH_3 and CH_4 adsorption

From Fig. 2, on Ni(211) and ZrNi(211), the most stable sites for CO and COH adsorptions are the Se-hcp sites with C atoms binding the surrounding three Ni atoms. The adsorption energies of CO and COH on Ni(211) are −2.00 and −4.42 eV, respectively; both are close to the adsorption energies of −2.10 and −4.50 eV on ZrNi(211), respectively. This indicates the negligible effect of Zr on the adsorption of CO and COH species.

Both C and CH species prefer to adsorb at the 4-hollow site on Ni(211) with four equal C—Ni bonds. When a Zr atom is substituted for a step Ni atom, the 4-hollow site made up of one Zr atom and three Ni atoms becomes completely unstable to accommodate C atoms with an elongated C—Zr bond and three shortened C—Ni bonds, thus, both C and CH species prefer to adsorb at the 4-hollow-Ni sites consisted of four Ni atoms. The adsorption energies of C and CH species on ZrNi(211) are −7.82 and −6.75 eV, which are rather close to the adsorption energies of −7.87 and −6.74 eV for C and CH on Ni(211), respectively; thus, the substituted Zr is far less attractive to C than Ni.

CH_2 prefers to adsorb at the Se-hcp and Se-hcp-Ni sites on Ni(211) and ZrNi(211), respectively. one of the H atoms sits above the neighboring Ni atom with the Ni–H distances of 1.799 and 1.675 Å on Ni(211) and ZrNi(211), respectively; the other H atom points out the surfaces; the adsorption energies of −4.13 and −4.25 eV for CH_2 on both surfaces are very close. Similarly, for CH_3, the C atom binds preferentially to Ni atoms, CH_3 prefers to adsorb at the Se-bridge and Se-bridge-Ni sites on both surfaces, respectively, the adsorption energies of −2.20 and −2.26 eV on Ni(211)

and ZrNi(211) are rather close, suggesting that the incorporation of Zr has no effect on the adsorption of CH_2 and CH_3 species.

CH_4 adsorbs preferentially at the Se-top and Se-top-Ni sites on Ni(211) and ZrNi(211), respectively. One of the C—H bonds is perpendicular to the surface, the other H atoms points towards the surface. The same weak adsorption energies of −0.02 eV on both surfaces indicate that the physisorption nature of CH_4 would easily desorb from the Ni surface once it is formed.

As shown in Fig. 2, CO, COH, C, CH, CH_2, CH_3 and CH_4 adsorb on Ni(211) and ZrNi(211) via C atom have almost the same site preference and structure characteristic; the adsorption energies of these species are much closer on both surfaces; suggesting that the adsorption of these species are not sensitive to surface structure.

3.1.3. O, OH, CH_3O, HCO, CH_2O, CH_2OH, CO_2, HCOH, H_2O and CH_3OH

For O adsorption, the Se-hcp-Zr site is energetically more favorable than the Se-hcp-Ni site on ZrNi(211), where the adsorption energy of O species is higher by 0.92 eV than that of −5.86 eV at the Se-hcp site on Ni(211), signifying that Zr is much more attractive to O rather than Ni.

Both OH and CH_3O species prefer to adsorb at the Se-bridge sites on Ni(211) with the adsorption energies of −3.86 and −2.90 eV, respectively. When Zr is introduced, the most favored sites for OH and CH_3O adsorption are changed to the Se-bridge-ZrNi sites, and the strong O—Zr bonds on this surface might be the reason for the significant increase of 0.85 and 0.93 eV for the adsorption energies of OH and CH_3O species, respectively.

HCO, CH_2O, CH_2OH and CO_2 species bind to the Se-bridge sites of Ni(211) via both O and C atoms anchoring at two adjacent Ni atoms, arranged in a similar way to the Se-bridge-ZrNi sites of ZrNi(211). However, these species bind the ZrNi(211) surface via the C—Ni and O—Zr bonds. In addition, for HCO, CH_2O, CH_2OH and CO_2, the adsorption energies on ZrNi(211) are increased by 0.96, 1.19, 0.76, 1.08 eV compared to those on Ni(211), respectively, suggesting that the substitution Zr tends to enhance the adsorption of oxygen species.

HCOH favors the adsorption of Se-bridge site via two C—Ni bonds on Ni(211) with an adsorption energy of −4.26 eV. However, when Zr is introduced, the most favored site of HCOH adsorption is changed to the Se-hcp-Zr site, in which HCOH binds to ZrNi(211) via both C—Ni and O—Zr bonds with a slight larger adsorption energy of −4.48 eV.

The geometries for H_2O adsorption on ZrNi(211), the planes of adsorbed H_2O molecule are nearly parallel to the surface, resembles that on Ni(211), in which H_2O is located at the Se-top site via O—Ni bond with an adsorption energy of −0.52 eV. As the incorporation of Zr into Ni stabilizes the O atom via the O—Zr bond, H_2O adsorption becomes more favorable with the large adsorption energy of −1.09 eV.

CH_3OH prefers to adsorb at the Se-top site on Ni(211) via O atom with an adsorption energy of −0.63 eV, and the C—O bond of CH_3OH is tilted relative to the normal of Ni(211). Interestingly, on ZrNi(211), CH_3OH initially sited at the Se-top-Ni site migrates to the nearest-neighbor Se-top-Zr site. However, when CH_3OH is posited at the Se-top-Zr site via O atom, the C—O bond of CH_3OH is activated and broken, in which CH_3 is far away from the surface, and the detached CH_3 fragment and the adsorbed OH has the stretched C—O distance of 3.077 Å from 1.452 Å in gas phase CH_3OH. Thus, CH_3OH is the dissociative adsorption state at the Se-top-Zr site on ZrNi(211), where the substitution of Zr is in favor of the C—O bond cleavage of CH_3OH. This agrees with the conclusions by Mori et al. [41,42], who provided a detailed analysis about the promoting effect of V, Mo, W, Nb and Re on the C—O bond dissociation rate of adsorbed CO in methanation on Ru/Al$_2$O$_3$, the main role of these promoters is to facilitate the C—O bond scission due to the interac-
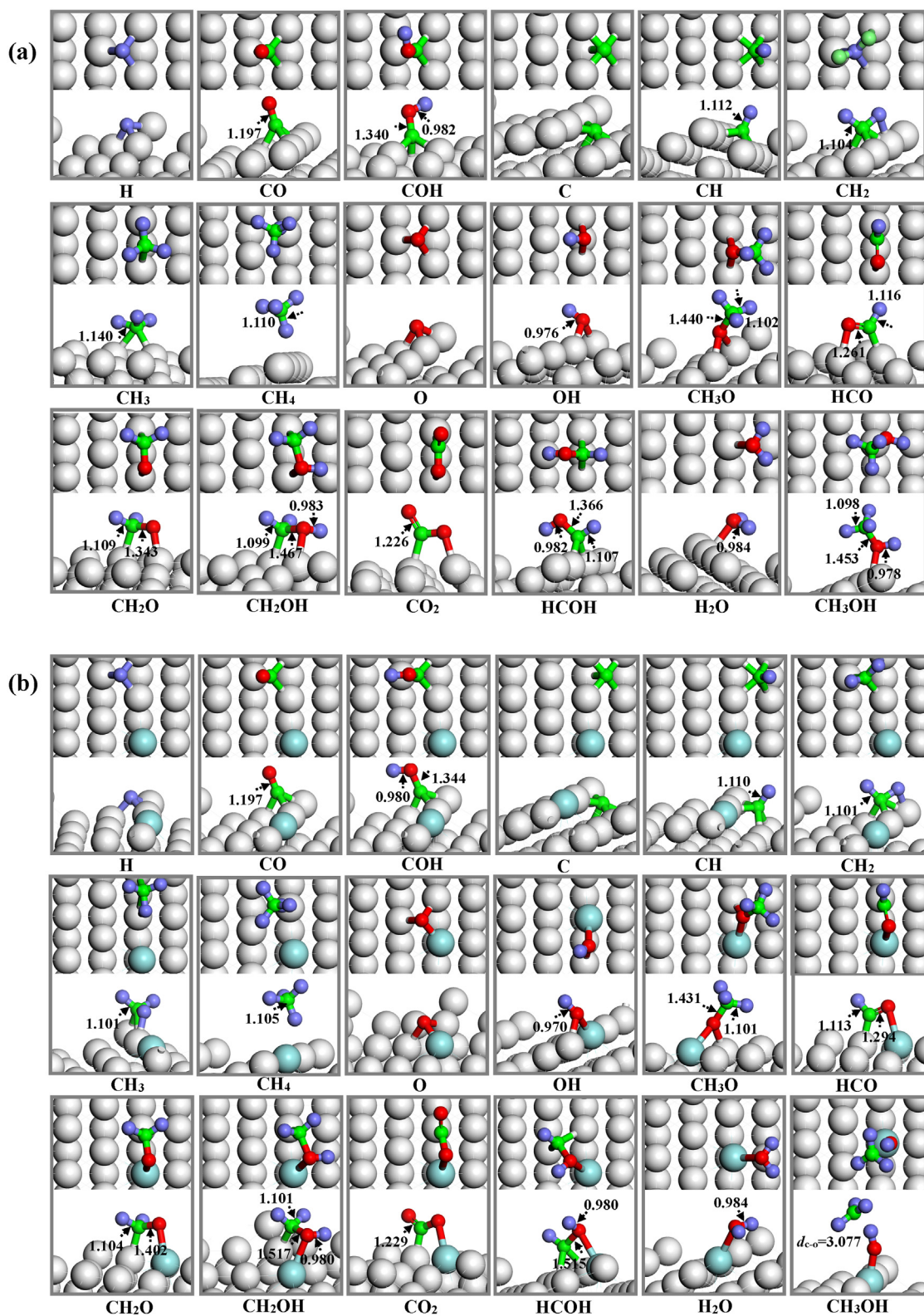
Fig. 2. The most stable configurations of the adsorbed species involved in CO methanation on (a) Ni(211) and (b) ZrNi(211) surfaces. The blue, gray, red, white and turquoise balls represent Ni, C, O, H and Zr atoms, respectively. (For interpretation of the references to colour in this figure legend, the reader is referred to the web version of this article.)

tion between the oxygen atom of chemisorbed CO and a positively charged promoter center [4,43].

As shown in Fig. 2, O, OH, CH_3O, HCO, CH_2O, CH_2OH, CO_2, HCOH, H_2O and CH_3OH tend to coordinate to Ni(211) and ZrNi(211) sur-

faces via O atoms with the O—Ni and/or O—Zr bonds, respectively. Notably, on ZrNi(211), O atoms of these species bind preferentially to Zr rather than Ni with the stronger Zr—O bonds. In addition, the adsorption energies of them on ZrNi(211) are obviously larger than

Table 1
Adsorption sites, adsorption energies (E_{ads}, eV) and the total charges (q) for the most stable adsorption configurations of the adsorbed species in CO methanation on Ni(211) and ZrNi(211) surfaces.

Species	Ni(211)			ZrNi(211)			Ni(111)[a]	Ni(211)[b]	Ni(211)[c]
	site	E_{ads}	q	site	E_{ads}	q	E_{ads}		
		eV			eV		eV		
H_2	Se-top	−0.18	−0.02	Se-top-Zr	−0.28	−0.02			
H	Se-hcp	−2.68	−0.31	Se-hcp-Ni	−2.74	−0.28	−2.78(fcc)	−2.86 (se-hcp)	−2.73 (se-hcp)
CO	Se-hcp	−2.00	−0.48	Se-hcp-Ni	−2.10	−0.50	−1.91(hcp)		−2.09 (se-hcp)
COH	Se-hcp	−4.42	−0.33	Se-hcp-Ni	−4.50	−0.35	−4.45(fcc)		−4.35 (se-hcp)
C	4-hollow	−7.87	−0.79	4-hollow-Ni	−7.82	−0.81	−6.82(fcc)	−7.98(4-hollow)	−7.45(4-hollow)
CH	4-hollow	−6.74	−0.62	4-hollow-Ni	−6.75	−0.63	−6.47(fcc)	−6.87(4-hollow)	−7.02(4-hollow)
CH_2	Se-hcp	−4.13	−0.42	Se-hcp-Ni	−4.25	−0.47	−4.07(fcc)	−4.39 (se-hcp)	
CH_3	Se-bridge	−2.20	−0.27	Se-bridge-Ni	−2.26	−0.31	−1.94(fcc)	−2.37(se-bridge)	
CH_4	Se-top	−0.02	−0.02	Se-top-Ni	−0.02	−0.04	−0.02(top)		
O	Se-hcp	−5.86	−0.90	Se-hcp-Zr	−6.78	−1.05	−5.76(fcc)		
OH	Se-bridge	−3.86	−0.53	Se-bridge-ZrNi	−4.71	−0.62	−3.54(fcc)		−3.47(se-bridge)
CH_3O	Se-bridge	−2.90	−0.52	Se-bridge-ZrNi	−3.83	−0.59	−2.75(fcc)		
HCO	Se-bridge	−2.50	−0.32	Se-bridge-ZrNi	−3.46	−0.55	−2.36(hcp)		−2.52(4-hollow)
CH_2O	Se-bridge	−1.13	−0.43	Se-bridge-ZrNi	−2.32	−0.70	−0.84(fcc)		
CH_2OH	Se-bridge	−2.11	−0.15	Se-bridge-ZrNi	−2.87	−0.33	−1.68(bridge)		
CO_2	Se-bridge	−0.42	−0.64	Se-bridge-ZrNi	−1.50	−0.80			−0.31
HCOH	Se-bridge	−4.26	−0.18	Se-hcp-Zr	−4.48	−0.24	−3.91(bridge)		
H_2O	Se-top	−0.52	0.03	Se-top-Zr	−1.09	−0.01	−0.33(top)		−0.72 (se-top)
CH_3OH	Se-top	−0.63	0.04	Se-top-Zr	dissociative adsorption		−0.37(top)		

[a] VASP code, GGA-PW91, 3×3 three-layer slab, $5 \times 5 \times 1$ k-points, energy cutoff of 340 eV [12] (ZPE corrections).
[b] VASP code, GGA-PW91, 2×4 five-layer slab, $5 \times 3 \times 1$ k-points, energy cutoff of 400 eV [40].
[c] SIESTA code, GGA-PBE, 2×1 twelve-layer slab, $3 \times 4 \times 1$ k-points, energy cutoff of 200Ry [11].

those on Ni(211), suggesting that the introduction Zr into Ni can stabilize these species.

3.2. CO methanation on Ni(211) and ZrNi(211) surfaces

Based on the adsorption behavior of the reaction intermediates on Ni(211) and ZrNi(211), the underlying mechanism of CO methanation have been investigated. To determine the reaction networks of CO methanation on Ni(211) and ZrNi(211) surfaces, all possible reaction pathways for various products in CO methanation have been examined (see Fig. 3). The activation energies (E_a) and reaction energies (ΔE) of the elementary reactions are listed in Table 2; the detailed discussions related to the elementary steps are presented in the Supplementary material.

3.2.1. The initial CO activation

Three reactions, CO direct dissociation into C + O, CO hydrogenation to COH or HCO, may occur for the initial CO activation, the potential energy diagram together with the structures of the initial state (ISs), transition state (TSs), and final states (FSs) are presented in Fig. 4.

As shown in Fig. 4(a), starting from the most stable CO adsorption configuration at the Se-hcp site, the direct C—O bond cleavage of CO on Ni(211) requires a significantly high activation energy of 3.02 eV, which is not kinetically favorable, and it agrees with the previous studies [7,8,11]. HCO formation is kinetically ($E_a = 1.24$ eV) favorable than COH formation ($E_a = 1.88$ eV); however, the former is highly endothermic ($\Delta E = 1.17$ eV), which may lead to a relatively low coverage over the metal surface, and hinder its further reactions. Hence, in this study, both HCO and COH intermediates have been considered in CO methanation on Ni(211).

As presented in Fig. 4(b), CO dissociation needs to overcome a large activation energy of 3.20 eV, which is higher than CO desorption energy of 2.10 eV, indicating that CO direct dissociation is also very difficult on ZrNi(211). HCO formation needs two steps., the first step is that the co-adsorbed CO and H first produce an intermediate *HCO-IM* via TS2-2, which is endothermic by 1.11 eV with an activation energy of 1.34 eV, and the generated *HCO-IM* adsorbs at the meta-stable Se-hcp-Ni site via two C—Ni bonds and one O—Ni bond;

the second step is that *HCO-IM* migrates from the meta-stable Se-hcp-Ni site ($E_{ads} = -2.52$ eV) to the most stable Se-bridge-ZrNi site ($E_{ads} = -3.46$ eV) via TS2-2′, which is exothermic by 0.84 eV with a very small activation energy of 0.22 eV. Thus, the overall activation energy of HCO formation is 1.34 eV, and it is only endothermic by 0.27 eV, which is favorable both thermodynamically and kinetically than the formation of COH ($E_a = 1.88$ eV; $\Delta E = 1.09$ eV). As a result, HCO is the dominant intermediate on ZrNi(211), suggesting that the promoter Zr can stabilize HCO species over Ni surface, and promote its further reactions. Therefore, different from Ni(211) surface, the reactions related to COH has not been considered in CO methanation on ZrNi(211).

3.2.2. CH_4 formation

The initial species, HCO and/or COH, undergo a series of hydrogenation and dissociation reactions to form $CH_x(x=0-3)$ and $H_xO(x=0,1)$, followed by the sequential hydrogenation to CH_4 and H_2O, respectively. The geometries of ISs, TSs and FSs involving in CO methanation to form CH_4, H_2O and CH_3OH on Ni(211) and ZrNi(211) surfaces are presented in Figs. 5 and 6, respectively. As a matter of fact, the overall activity of CH_4 formation via the H-assisted CO dissociation pathway may be controlled by all different steps, as presented in Fig. 3, in which CH_4 formation involves the bond-cleavage (C—O) and bond-formation (C—H and O—H) steps, as pfollows:

Paths	Ni(211)	ZrNi(211)
CO → HCO → CH → CH_2 → CH_3 → CH_4	Path1–1	Path 2–1
CO → HCO → HCOH → CH → CH_2 → CH_3 → CH_4	Path 1–2	Path 2–2
CO → HCO → HCOH → CH_2OH → CH_2 → CH_3 → CH_4	Path 1–3	Path 2–3
CO → HCO → CH_2O → CH_2 → CH_3 → CH_4	Path 1–4	Path 2–4
CO → HCO → CH_2O → CH_2OH → CH_2 → CH_3 → CH_4	Path 1–5	Path 2–5
CO → HCO → CH_2O → CH_3O → CH_3 → CH_4	Path 1–6	Path 2–6
CO → COH → C → CH → CH_2 → CH_3 → CH_4	Path 1–7	Path 2–7
CO → COH → HCOH → CH → CH_2 → CH_3 → CH_4	Path 1–8	–
CO → COH → HCOH → CH_2OH → CH_2 → CH_3 → CH_4	Path 1–9	–

The potential energy diagram of all reaction pathways leading to CH_4 and H_2O on Ni(211) and ZrNi(211) are presented in Figs. S1 and S2 in the Supplementary material, respectively. We can obtain that the energetically favorable pathways to form CH_4 are indentified as Path 1–7 and Path 1–9 on Ni(211) and Path 2–5 on ZrNi(211).
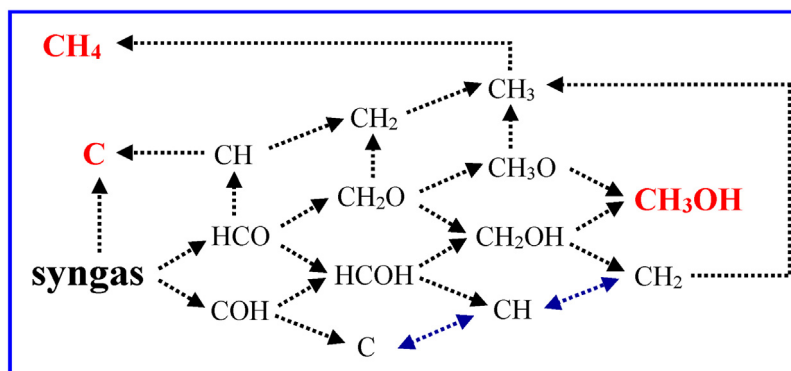
Fig. 3. Reaction network involving in CO methanation to form CH_4, CH_3OH and C on Ni(211) and ZrNi(211) surfaces.

Table 2
Activation energies (E_a) and reaction energies (ΔE) of all possible elementary reactions, as well as the only one imaginary (v) of transition states involved in CO methanation on Ni(211) and ZrNi(211) surfaces.

Reaction		Ni(211)				ZrNi(211)				Ni(111)[a]	Ni(211)[b]
		E_a	ΔE	v		E_a	ΔE	v		E_a	
		(eV)		cm^{-1}		(eV)		cm^{-1}		(eV)	
$CO \to C + O$	R1-1	3.02	0.08	395 i	R2-1	3.20	−0.71	425 i		3.71	2.95
$CO + H \to HCO$	R1-2	1.24	1.17	304 i	R2-2	1.34	1.11	540 i		1.42	1.46
					R2-2′	0.22	−0.84	30 i			
$CO + H \to COH$	R1-3	1.88	1.12	1537 i	R2-3	1.88	1.09	1500 i		1.95	1.82
$HCO \to CH + O$	R1-4	1.27	−0.80	447 i	R2-4	1.36	−0.67	223 i		1.15	
$CH + H \to CH_2$	R1-5	0.93	0.59	296 i	R2-5	1.49	0.52	508 i		0.76	
$CH_2 + H \to CH_3$	R1-6	0.39	−0.13	823 i	R2-6	0.74	−0.13	774 i		0.78	
$CH_3 + H \to CH_4$	R1-7	0.81	0.36	863 i	R2-7	1.02	0.39	1011 i		1.00	
$O + H \to OH$	R1-8	1.04	−0.10	1092 i	R2-8	1.18	−0.01	1298 i		1.21	1.16
$OH + H \to H_2O$	R1-9	1.38	0.66	869 i	R2-9	1.21	1.07	1097 i		1.32	
$HCO + H \to HCOH$	R1-10	1.16	0.40	1348 i	R2-10	1.72	1.25	1325 i		0.90	
$HCOH \to CH + OH$	R1-11	1.12	−1.07	455 i	R2-11	0.49	−1.66	64 i		0.74	
$HCOH + H \to CH_2OH$	R1-12	0.46	0.33	173 i	R2-12	0.53	−0.35	974 i		0.90	
$CH_2OH \to CH_2 + OH$	R1-13	0.27	−0.70	51 i	R2-13	0.01	−0.80	28 i		0.74	
$CH_2OH + H \to CH_3OH$	R1-14	0.65	0.20	843 i							
$HCO + H \to CH_2O$	R1-15	0.65	0.34	813 i	R2-15	0.74	0.09	876 i		0.62	
$CH_2O \to CH_2 + O$	R1-16	1.01	−0.26	537 i	R2-16	1.29	−0.14	66 i		1.30	
$CH_2O + H \to CH_2OH$	R1-17	1.07	0.27	1304 i	R2-17	1.23	0.77	1297 i		1.03	
$CH_2O + H \to CH_3O$	R1-18	0.41	−0.09	28 i	R2-18	0.77	0.15	922 i		0.67	
$CH_3O \to CH_3 + O$	R1-19	1.25	−0.30	510 i	R2-19	1.55	−0.27	590 i		1.45	
$CH_3O + H \to CH_3OH$	R1-20	1.39	0.65	702 i						1.23	
$COH \to C + OH$	R1-21	1.10	−0.97	116 i	R2-21	2.02	−1.67	422 i		2.01	1.03
$C + H \to CH$	R1-22	0.70	0.35	651 i	R2-22	0.77	0.32	666 i			
$COH + H \to HCOH$	R1-23	0.76	0.52	160 i							
$CH_2 \to CH + H$	R1-24	0.40	−0.59	281 i	R2-24	0.99	−0.52	654 i			
$CH \to C + H$	R1-25	0.35	−0.35	661 i	R2-25	0.45	−0.32	664 i		1.38	0.75
$CO + CO \to C + CO_2$	R1-26	3.70	1.02	268 i	R2-26	2.83	0.12	418 i			
$C + C \to C_2$	R1-27	1.86	0.42	149 i	R2-27	1.47	0.37	364 i			

^a VASP code, GGA-PW91, 3 × 3 three-layer slab, 5 × 5 × 1 k-points, energy cutoff of 340 eV [12].
^b SIESTA code, GGA-PBE, 2 × 1 twelve-layer slab, 3 × 4 × 1 k-points, energy cutoff of 200Ry [11].

The corresponding overall activation energies are 2.22 and 2.24 eV on Ni(211) and 1.59 eV on ZrNi(211), as shown in Figs. 5 and 6, respectively.

On Ni(211), COH direct dissociation to C and OH is significantly exothermic by 0.97 eV, the corresponding E_a is 1.10 eV, which is much lower than CO direct dissociation (E_a = 3.02 eV). Clearly, the C—O bond length in COH (1.340 Å) is longer than that in CO (1.197 Å), suggesting that the C—O bond is pre-activated and obviously weaken by the initial CO hydrogenation. This is why H-assisted CO activation is more energetically favorable compared to CO direct dissociation. Starting from C species, C species undergoes the sequential hydrogenation reactions to form CH_4, as shown in Path 1–7 (see Fig. 5); the formations of CH and CH_2 are endothermic by 0.35 and 0.60 eV, respectively; CH_3 formation is slightly exothermic by 0.14 eV. The activation energies of CH, CH_2, CH_3 and CH_4

formation are 0.70, 0.93, 0.39 and 0.81 eV, respectively, which agree with the previous studies (see Table 2).

Meanwhile, COH hydrogenation is also considered as a possible route to form CH_4 on Ni(211), as shown in Path 1–9 (see Fig. 5), both HCOH or CH_2OH formations is endothermic by 0.52 eV and 0.33 eV, respectively; the corresponding activation energies are 0.76 and 0.46 eV. The C—O bond cleavage of CH_2OH leads to CH_2 and OH with an activation energy of 0.27 eV; then, CH_2 is successively hydrogenated to form CH_4.

On ZrNi(211), HCO undergoes two hydrogenations to form CH_2OH via CH_2O intermediates, as shown in Path 2–5 (see Fig. 6). CH_2O formation is endothermic by 0.09 eV with an activation energy of 0.74 eV. CH_2OH formation is also endothermic by 0.77 eV with the activation energy of 1.23 eV. The C—O bond cleavage of CH_2OH can form CH_2 and OH, this elementary reaction is exother-
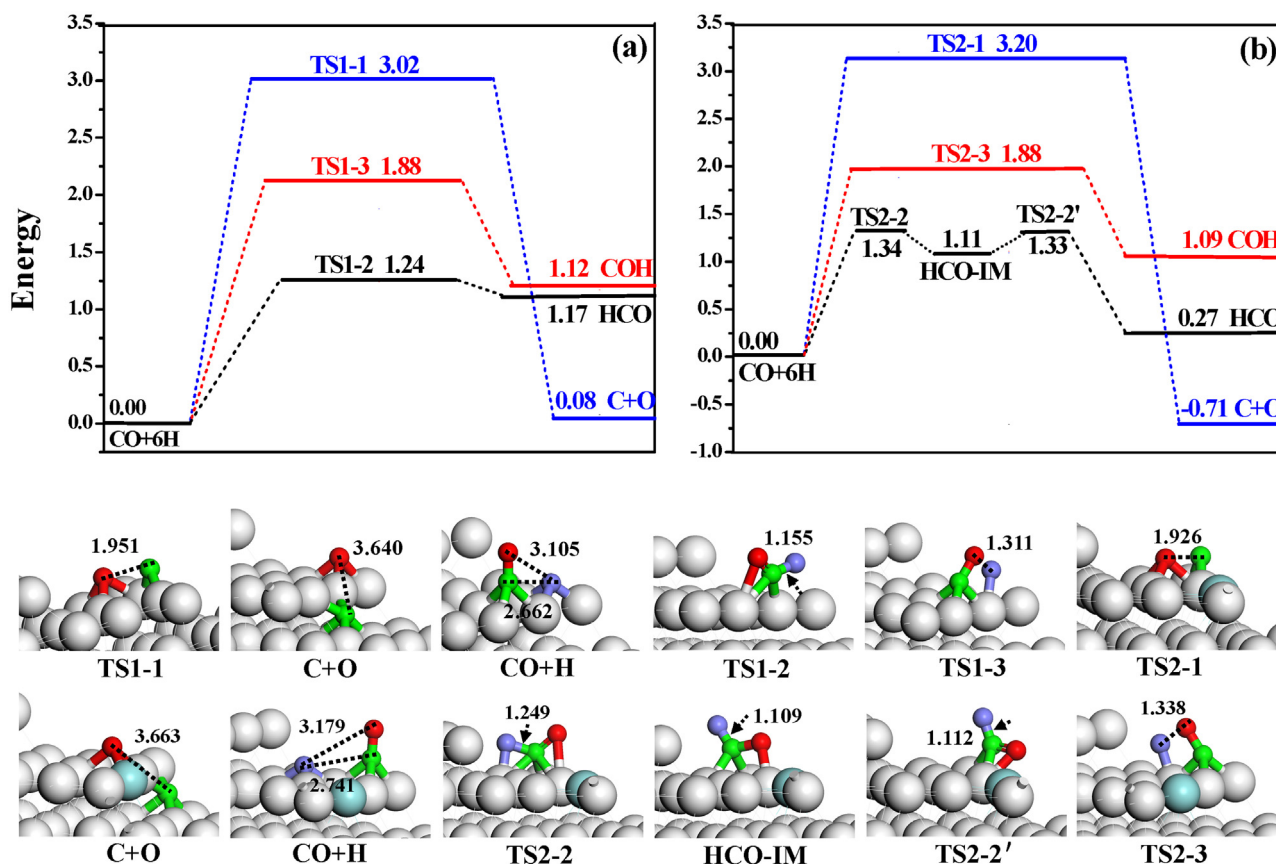
Fig. 4. The potential energy diagram of the initial CO activation together with the corresponding structures on (a) Ni(211) and (b) ZrNi(211) surfaces. Bond lengths are in Å. See Fig. 2 for color coding.

mic by 0.80 eV with a very small activation energy of 0.01 eV; further, CH_2 undergoes the successive hydrogenations to form CH_4.

On the other hand, H_2O may be also formed in CO methanation, OH is produced via the C−O bond cleavage of COH and/or CH_2OH on Ni(211) and ZrNi(211), respectively; OH hydrogenation to H_2O is endothermic by 0.66 and 1.07 eV, respectively; the corresponding activation energies are 1.38 and 1.21 eV, respectively.

Above results show that the direct and H-assisted COH dissociation on Ni(211) surface have the lower overall barrier compared to other H-assisted CO pathways, which agrees with the studies by Andersson et al. [8], suggesting that CO dissociation proceeds most favorably via COH species over under coordinated sites, and COH is thought to be a key intermediate. Moreover, the overall barrier for the most favorable pathway of CH_4 formation (1.59 eV in Path2-5) on ZrNi(211) is much lower than those (2.22 eV in Path1-7 and 2.24 eV in Path1-9) on Ni(211), suggesting that the incorporation of Zr into Ni can enhance the catalytic activity toward CH_4 formation.

3.2.3. The effect of CH_3OH formation on CH_4 formation

On Ni(211), once CH_2OH and/or CH_3O are formed, both can hydrogenate to form CH_3OH. The activation energy of CH_2OH hydrogenation to CH_3OH is higher by 0.38 eV than that for the C−O bond scission to form CH_2 and OH, suggesting that CH_2OH prefers to dissociate into CH_2, followed by the successive hydrogenations to form CH_4 rather than being hydrogenated to CH_3OH. Again, the activation energy of CH_3O hydrogenation to CH_3OH is higher by 0.14 eV than that for the C−O bond scission of CH_3O, namely, CH_3O hydrogenation to CH_3OH can be hindered by CH_3O dissociation into O and CH_3, followed by hydrogenation to CH_4. As a result, the stepped Ni(211) surface exhibits a higher selectivity toward CH_4 formation rather than CH_3OH.

On ZrNi(211), as mentioned in Section 3.1.3, CH_3OH is the dissociative adsorption, the C−O bond cleavage of CH_3OH results in CH_3, followed by its hydrogenation to CH_4. Moreover, in the most favorable pathway of CH_4 formation, the C−O bond cleavage of CH_2OH leading to $CH_2 + OH$ only need a very small activation energy of 0.01 eV, this step is strongly exothermic by 0.80 eV, Thus, CH_3OH is hardly formed on ZrNi(211).

3.2.4. Microkinetic modeling

Although the overall activity and selectivity of CH_4 and CH_3OH formation via the H-assisted CO dissociation pathways on Ni(211) can be controlled by the relative activity between the hydrogenation and dissociation of CH_2OH, it is quite incomplete only based on the rate constant. A microkinetic modeling is necessary to estimate the selectivity of CH_4 and CH_3OH under the experimental conditions [1–5,8], and this microkinetic modeling has been successfully applied in various reactions [8,44,45]. The detailed description of microkinetic model is depicted in Part 2 of the Supplementary material; the pseudo-steady-state approximation is employed to the surface species except for CO and H_2, the adsorption processes are assumed to be equilibrium. The rate constants of all elementary reactions involved in CH_4 formation from syngas at the temperatures of 550, 575, 600, 625, 650, 675, 700, 725 and 750 K are listed in Table S2 in the Supplementary material. According to the rate constants of the relevant elementary reactions and the microkinetic model, the rates of r_{CH_4} and r_{CH_3OH}, as well as the relative selectivity of the major productions between CH_4 and CH_3OH at the different temperatures are presented in Table S3 in the Supplementary material and Fig. 9, respectively. Here, the relative selectivity is defined by the relative rate for each product, $r_i/(r_{CH_4} + r_{CH_3OH})$, where i is the species of the products.
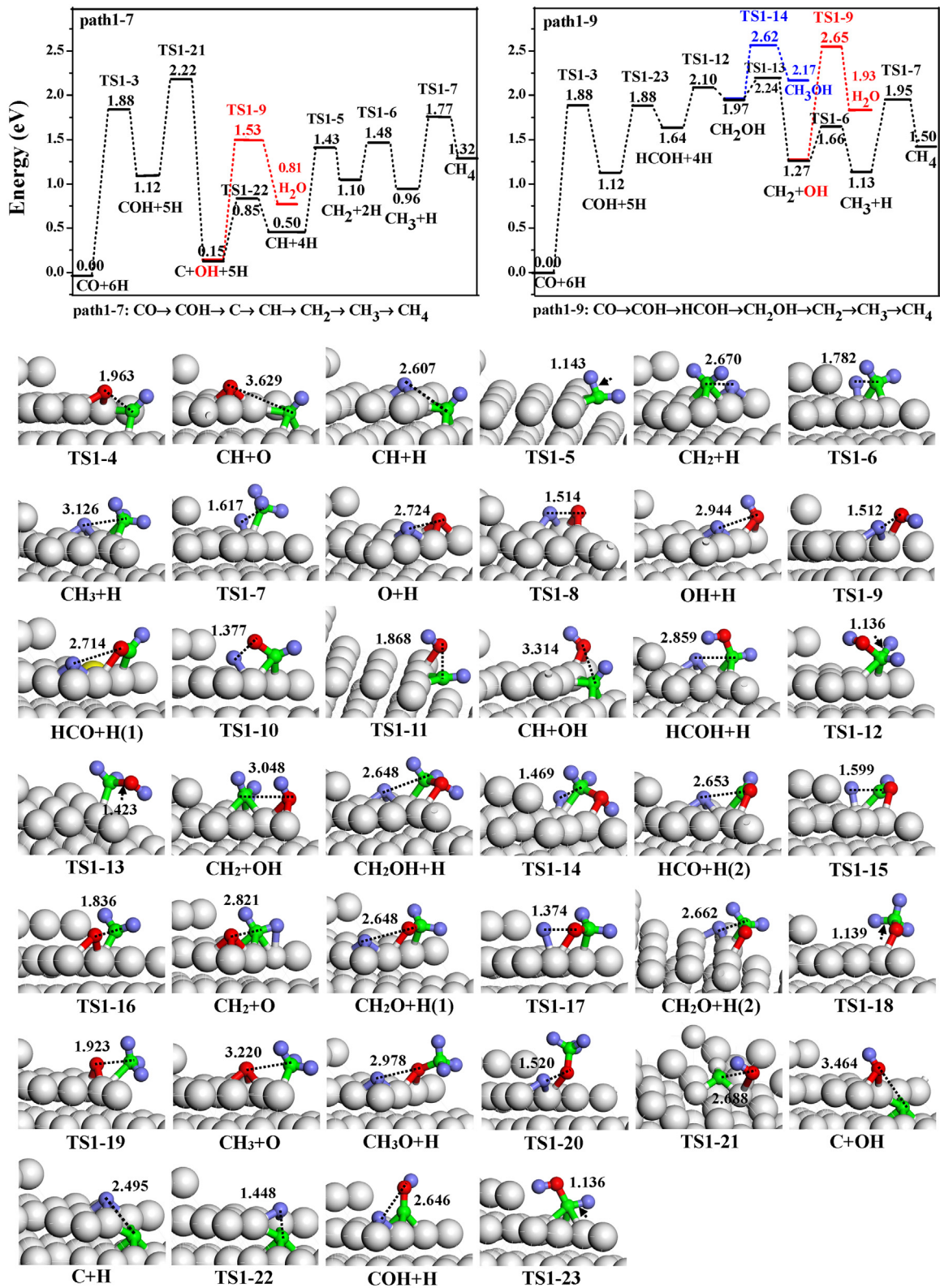
Fig. 5. The potential energy diagram of the energetically favorable pathways for CH_4 formation together with the structures of the initial states, transition states and final states involving in CO methanation to form CH_4, H_2O and CH_3OH on Ni(211) surface. Bond lengths are in Å. See Fig. 2 for color coding.

As shown in Fig. 9, the relative selectivity of CH_4 is higher than that of CH_3OH at the same temperatures. With the increase of temperature from 550 to 750 K, the relative selectivity of CH_4 are greater than 78% and gradually increase to the stable value of approximately 99%, which is much higher than that of CH_3OH.

Meanwhile, the relative selectivity of CH_4 using the microkinetic modeling agrees well with the experiment result [1–5,8]. Moreover, the variation trend of the relative selectivity of CH_3OH is opposite to that of CH_4, the relative selectivity of CH_3OH decrease significantly with the increase of temperature, which means that the stepped
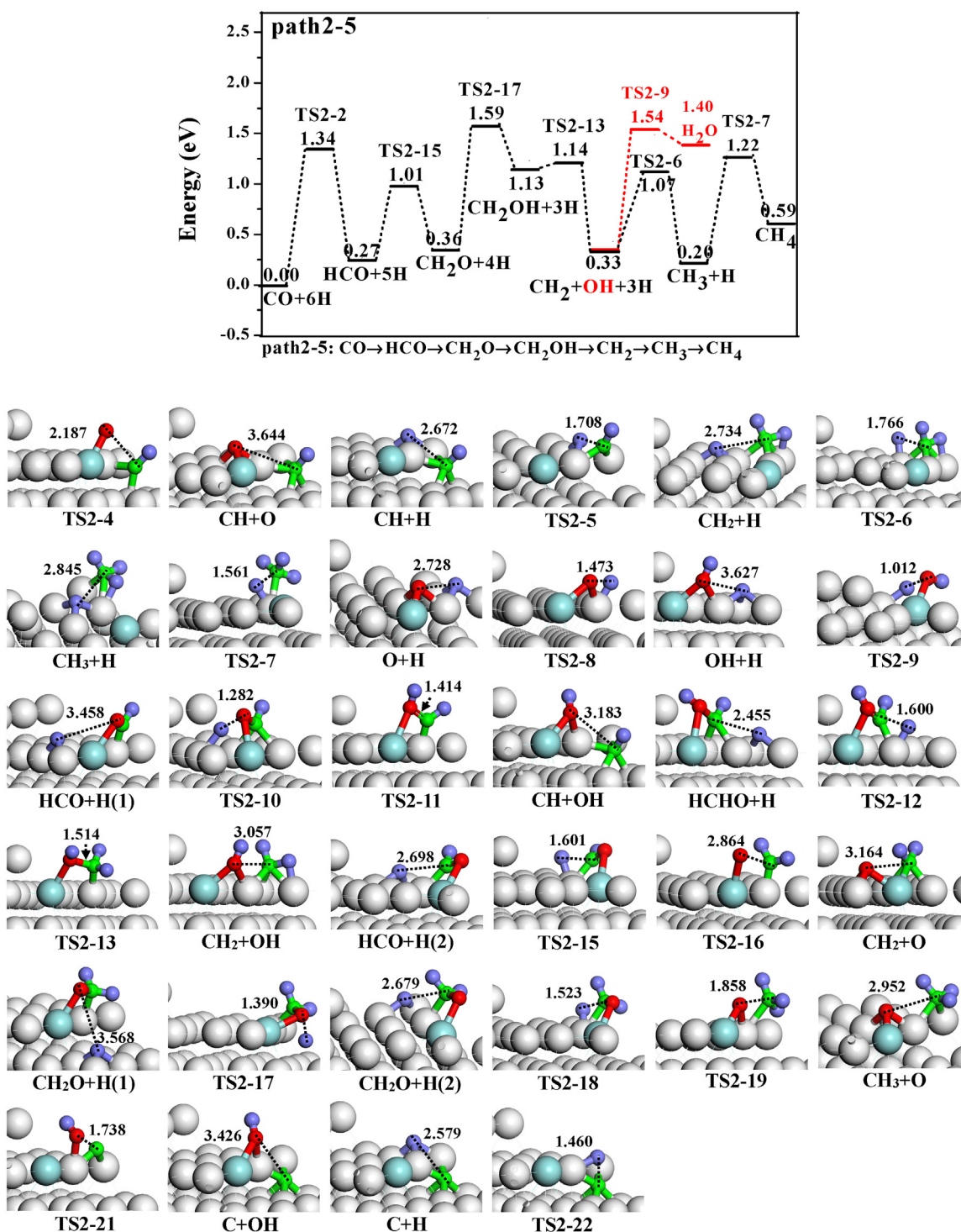
Fig. 6. The potential energy diagram of the energetically favorable pathway for CH_4 formation together with the structures of the initial states, transition states and final states involving in CO methanation to form CH_4 and H_2O on ZrNi(211) surface. Bond lengths are in Å. See Fig. 2 for color coding.

Ni(211) surface can effectively improve CH_4 selectivity rather than CH_3OH.

3.3. Carbon formation and elimination on Ni(211) and ZrNi(211) surfaces

3.3.1. Carbon formation from CO

$CO \rightarrow C + O$ and $CO + CO \rightarrow CO_2 + C$ may occur for carbon formation on Ni(211) and ZrNi(211) surfaces in CO methanation, as listed in Table 2 (R1-1, R1-26, R2-1, R2-26). The potential energy profile together with the structures of ISs, TSs and FSs are provided in Fig. 7.

$CO \rightarrow C + O$ reaction has the high E_a of 3.02 and 3.20 eV on Ni(211) and ZrNi(211), respectively; $CO + CO \rightarrow CO_2 + C$ reaction describes CO disproportionation that occurs at high CO surface coverage on metal surface, the corresponding activation barriers are 3.70 and 2.83 eV on Ni(211) and ZrNi(211), respectively, which are close to the previously reported value (3.48 eV) on Ni(111) [12]. As
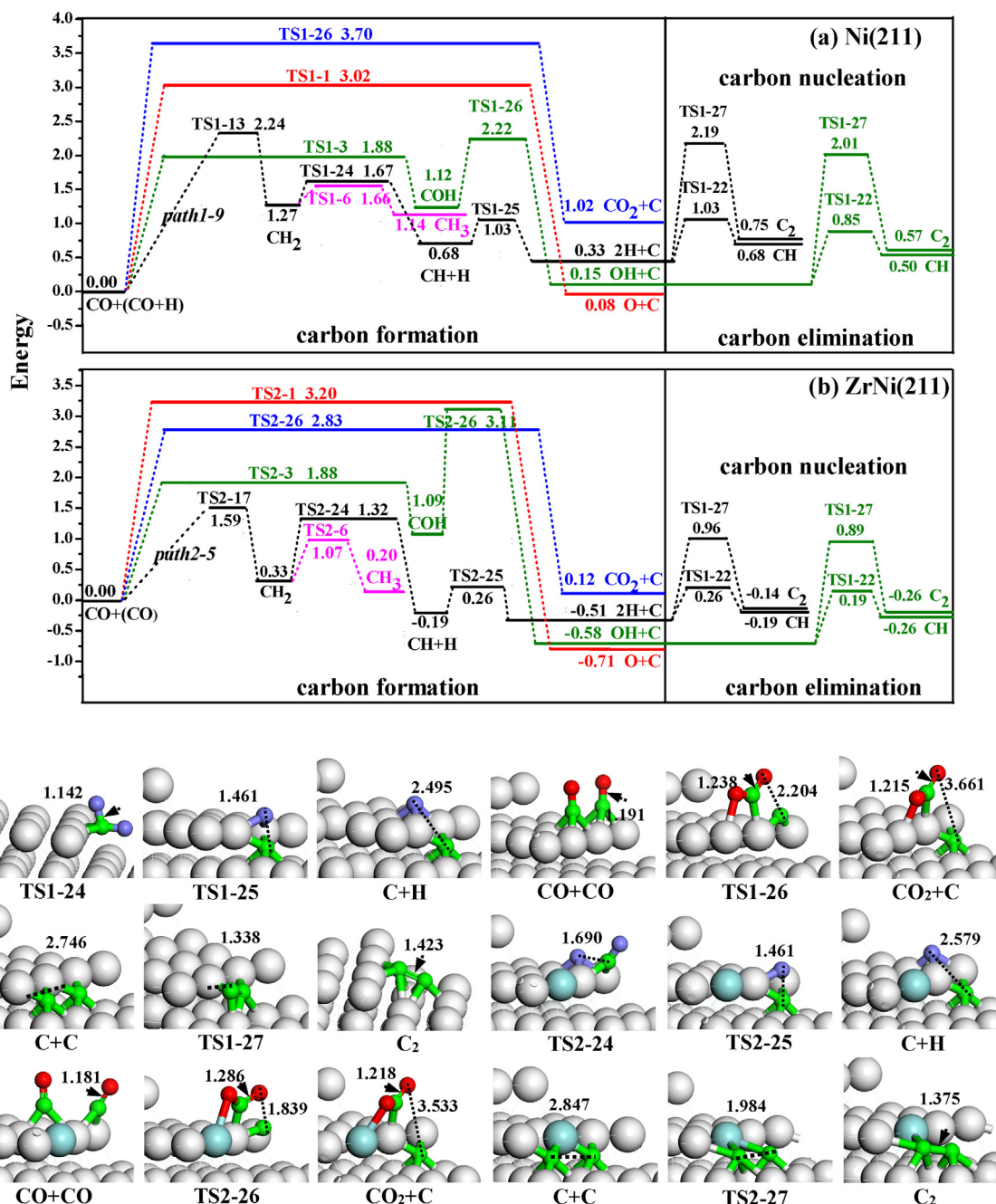
Fig. 7. The potential energy profile of all possible reactions leading to carbon formating and eliminating on (a) Ni(211) and (b) ZrNi(211) surfaces together with the corresponding structures. Bond lengths are in Å. See Fig. 2 for color coding.

a result, carbon formation on these three Ni surfaces is unlikely to occur due to the higher activation energy.

3.3.2. Carbon formation from the pathway of CH_4 formation on Ni(211) surface

As mentioned above, Path 1–7 and Path 1–9 are mainly responsible for CH_4 formation on Ni(211). In *Path 1–7*, carbon formation ascribes to the C—O bond cleavage of COH; and in *Path 1–9*, CH_2 species is the dominant CH_x monomer in CO methanation. As shown in Fig. 7(a), the sequential dehydrogenation of CH_2 is identified as the source of carbon formation, the hydrogenation and dissociation of CH_2 is competitive. Thus, carbon deposition is more likely to occur in the vicinity of the step Ni site. Further, large amounts of carbon deposition on Ni surface will eventually poison

the steps. This result confirms the facts that the stepped Ni(211) is much susceptible to deactivation by coke [11].

3.3.3. The effect of Zr promoter on carbon formation

As shown in Fig. 7(b), Path 2–5 is mainly responsible for CH_4 formation on ZrNi(211), in which CH_2 is the common intermediate, E_a of CH_2 dehydrogenation is higher by 0.25 eV than that of CH_2 hydrogenation. Thus, the subsequent CH_2 dehydrogenation is hindered by the high E_a, indicating that Zr promoter is effective in tuning the selectivity of CH_4. This agrees with the experiment conclusions [1–5] that adding Zr into Ni catalyst can increase the productivity and selectivity of CH_4, as well as the resistance to coke deposition. Interestingly, it can be seen that coke deposition is expected to dominantly take place on Ni(211). Once Zr is doped into Ni cata-
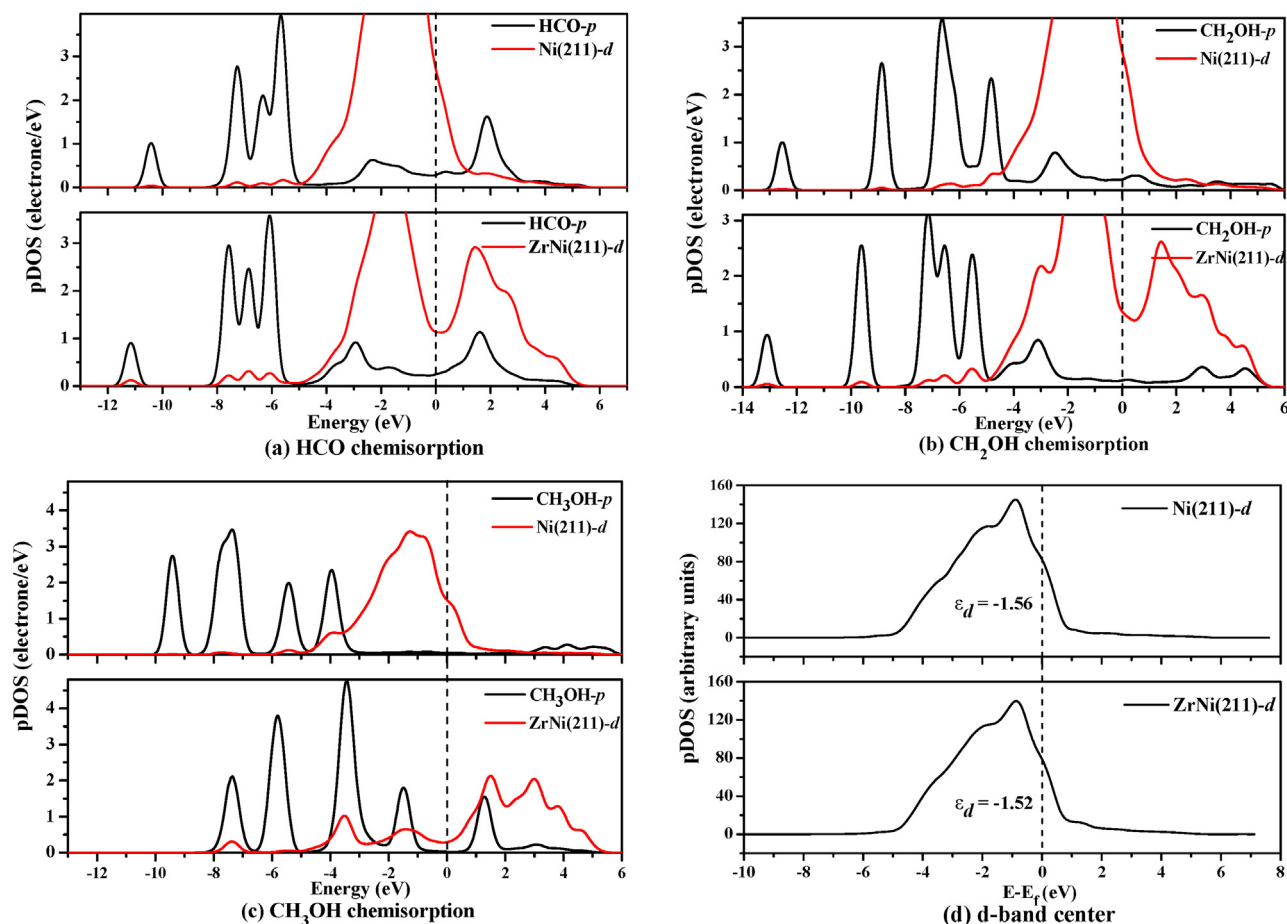
Fig. 8. Projected density of states (pDOS) for (a) HCO, (b) CH$_2$OH (c) CH$_3$OH chemisorptions, and (d) *d*-band center on Ni(211) and ZrNi(211) surfaces. The vertical line indicates the Fermi level.
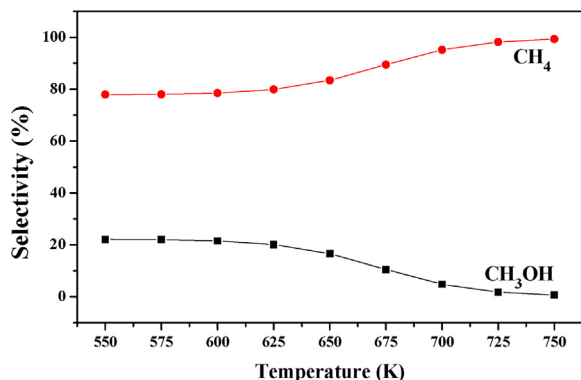

Fig. 9. The relative selectivity of products CH$_4$ and CH$_3$OH from the syngas reaction on Ni(211) at different temperatures using the microkinetic modeling technique.

lyst, carbon formation is significantly suppressed since CH$_2$ prefers to be hydrogenated to CH$_3$ rather than being dehydrogenated into CH.

3.3.4. The elimination and nucleation of carbon corresponding to C + H → CH and C + C → C$_2$

Two reactions of C + H → CH and C + C → C$_2$ correspond to carbon elimination and carbon nucleation on Ni(211) and ZrNi(211), respectively; as listed in Table 2 (R1-22, R1-27, R2-22, R2-27), and the potential energy profile along with the ISs, TSs and FSs are provided in Fig. 7.

The nucleation of two isolated C atoms produce C$_2$ dimmer via R1-27 and R2-27 on Ni(211) and ZrNi(211), respectively; the reactions begin with one C atom leaving the 4-hollow site and moving to the bridge site with a shorted C—C distance, as shown in Fig. 7. After their respective transition state of TS1-27 and TS2-27, the left C atoms arrive at the Ni edge, and two isolated C atoms eventually agglomerate to form a C$_2$ dimmer. C + C → C$_2$ reactions are calculated to be endothermic by 0.42 and 0.37 eV on Ni(211) and ZrNi(211), respectively; the corresponding E_a are 1.86 and 1.37 eV, respectively. The reverse step of C—C bond scission to two separated C atoms have been investigated [46], suggesting that the formation of C$_2$ dimmer is endothermic by 0.63 eV with a E_a of 1.89 eV. Hence, the unwanted coke deposition may occur only when carbon centers are completely dehydrogenated but not removed from the catalyst surface [47].

Interesting, carbon is found to react preferentially with H atom rather than C + C → C$_2$ reaction on Ni(211), in which carbon hydrogenation via R1-22 and carbon nucleation via R1-27 corresponds to a large difference of activation barrier by >1 eV. A similar trend is found that carbon prefers to hydrogenate to CH via R2-22 rather than C + C → C$_2$ via R2-27 on ZrNi(211), namely, carbon formation at the step is expected to eliminated by hydrogenation.

The same is true for the activation barrier of C hydrogenation with or without Zr at the step; the observed carbon deposited as the reactants are pumped out on both surfaces. Therefore, if there is an occurrence of carbon deposition, which could be alleviated by increasing H$_2$/CO ratio [48]. The finding is clearly in accordance with the results that carbon is not an efficient poison for the methanation process at low CO coverage, whereas, sulphur poison-

ing and Ni sintering turn out to be of great importance [8,49]. To provide auxiliary functions, such as sulphur-resistance, sintering-resistance and carbon-resistance properties, extensive efforts by probing into the combinations of more effective promoters will be considered in our next work. This topic is out of the scope of the current work.

3.4. General discussions

3.4.1. The effect of surface structure on activity and selectivity of CH$_4$ formation between Ni(211) and Ni(111)

Our results summarized in Fig. 5 show that Path 1–7 and Path 1–9 are kinetically feasible for CH$_4$ formation on Ni(211), with the overall activation energies of 2.22 and 2.24 eV, respectively; which is comparable to the previous results [12] on Ni(111) that two parallel pathways of CO → HCO (or HCO → HCOH) → CH → CH$_2$ → CH$_3$ → CH$_4$ dominantly contribute to CH$_4$ formation with the value of 0.30 or 0.33 eV, respectively. The overall activation energies are reduced by 0.1 eV due to the promotional effect of the stepped Ni(211) on CH$_4$ formation, suggesting that surface structure of Ni catalyst can enhance the catalytic activity of CH$_4$ formation, which agrees with the previous studies [8] that CO conversion to CH$_4$ via the COH intermediate on the stepped Ni(211) surface, is feasible and more favorable than that on the flat Ni(111) surface.

The flat terrace of Ni(111) has the high overall activation energy of 2.30 or 2.33 eV for CH$_4$ formation, as mentioned above, which is kinetically less favorable than the competitive CH$_3$OH formation with the value of 2.36 eV. Therefore, the flat Ni(111) is not expected to be an efficient surface to improve the selectivity of CH$_4$. It can be seen that the stepped Ni(211) surface would obviously improve the selectivity of CH$_4$ in CO methanation, and provide a more favorable pathway for CH$_4$ formation. Hence, the stepped Ni(211) surface exhibits the higher catalytic activity and selectivity toward CH$_4$ formation rather than CH$_3$OH, which is also supported by the fact that the steps completely control the reactivity of CO methanation [8].

3.4.2. The effect of surface composition on activity and selectivity of CH$_4$ formation between Ni(211) and ZrNi(211)

Above results show that the stepped Ni(211) surface exhibit a superior selectivity toward CH$_4$ formation over the flat Ni(111) surface, while the effect of surface structures on the activity of CH$_4$ formation is rather small. In the case of a more active Zr atom embedded to a less active Ni(211), the situation is significant imporved. Thus, the comparisons between Ni(211) and ZrNi(211) have been further carried out to probe into the effect of surface composition on the activity and selectivity of CH$_4$ formation.

As shown in Fig. 6, Path 2–5 dominantly contributes to CH$_4$ formation on ZrNi(211), moreover, the overall activation energy of 1.59 eV on ZrNi(211) are much lower than those (2.22 and 2.24 eV) on Ni(211), indicating that CH$_4$ formation on ZrNi(211) is much more favorable than that on Ni(211). On the other hand, the effect of Zr promoter on CH$_3$OH formation is of particular interest, CH$_3$OH is the dissociative adsorption state on ZrNi(211), the C−O bond cleavage of CH$_3$OH results in CH$_3$, followed by its hydrogenation to CH$_4$; namely, no CH$_3$OH yield is expected on ZrNi(211).

Thus, compared to the pure Ni(211) and Ni(111) surfaces, ZrNi(211) exhibits the higher activity and selectivity toward CH$_4$ formation, namely, the promoter Zr not only facilitate CH$_4$ formation, but also eliminate the undesirable product such as CH$_3$OH.

3.4.3. The role of Zr for CH$_4$ formation

Compared to Ni(211), ZrNi(211) exhibits a higher catalytic activity and selectivity toward CH$_4$ formation, indicating that the promoter Zr at a step site can render the steps more active than Ni at a step site.

The main role of Zr is that, firstly, throughout the whole reaction network, it is found that the initial CO activation to HCO occurs at the step Ni site, subsequently, the generated HCO can easily migrates to the step Zr site due to the lower activation energy and the larger HCO stabilization. This extremely decreases the overall activation energy of CH$_4$ formation. As a result, the presence of promoter Zr greatly facilitates the cleavage of C−O bond of CH$_2$OH, and promotes CH$_2$ formation, results in a significant increase of the reaction activity.

Secondly, CH$_3$OH is the dissociative adsorption at the step Zr site, the C−O bond cleavage of CH$_3$OH results in CH$_3$, followed by its hydrogenation to CH$_4$, consequently, no CH$_3$OH is formed when Zr is doped. This leads to a superior selectivity to CH$_4$ in CO methanation.

Thirdly, by introducing Zr, a significant carbon-deposition resistance is observed, the principal reason is that CH$_2$, the dominant existence form of CH$_x$, is more likely to hydrogenate to CH$_4$, comparative to the dehydrogenation to carbon.

Thereby, the enhanced activity and selectivity toward CH$_4$, as well as carbon-deposition resistance on ZrNi(211) surface mainly originated from the Zr step site, where the synergistic effect between Zr and Ni plays an important role.

3.4.4. Electronic structure analysis the role of Zr promoter for CH$_4$ formation

According to foregoing analysis, the promoter Zr can not only stabilize HCO but also facilitate the cleavage of C−O bond of CH$_2$OH, especially for CH$_3$OH, the C−O bond cleavage happen spontaneously. To further clarify the effect of Zr promoter on CH$_4$ formation, the projected density of states (pDOS) [50] and Bader charges analysis [51] have been examined.

As listed in Table 1, the increase of charge density for HCO, CH$_2$OH and CH$_3$OH is obtained from ZrNi(211) compared to that from Ni(211), which agrees with the pDOS analysis, as presented in Fig. 8(a)–(c), the d orbital of Zr greatly overlaps with the p orbital of O atom, while the hybridization is not distinct between the d orbital of Ni and the p orbital of O atom. This indicates that the promoter Zr results in the strong interaction between these oxygenates and the substrate. This statement is further supported by the upshift of the average energy of the d-band (ε_d) of ZrNi(211) surface, which is calculated by the Eq. (10).

$$\varepsilon_d = \frac{\int_{-\infty}^{E_f} E\rho_d(E)\,dE}{\int_{-\infty}^{E_f} \rho_d(E)\,dE} \tag{10}$$

where ρ_d represents the density of states projected onto the Ni(Zr) atoms' d-band; E is the energy of d-band. As seen in Fig. 8(d) using PW91 functional, a shift of ε_d of ZrNi(211) to higher energy leads to more anti-bonding states being emptied and strengthens the interaction between Zr and O, and thereby leads to an increase of the reactivity. The comparisons between the d-band center calculated using GGA + U approach [52] and that obtained by GGA/PW91 functional on Ni(211) and ZrNi(211) have been carried out, as presented in Table S4 and Fig. S3 in Part 3 of the Supplementary material, the same results about the promotional effect of Zr doping on Ni(211) can be obtained. Conclusively, the strong interaction between the positively charged Zr and O enhances the adsorption ability of HCO, promotes the C−O bond cleavage of CH$_2$OH and CH$_3$OH, and thereby leads to a significant increase of the activity and selectivity of CH$_4$ formation due to the electronic effect.

4. Conclusions

In this study, DFT calculations have been employed to probe into the effects of the surface structure and composition on the activity and selectivity of CO methanation on Ni(211) and ZrNi(211)

surfaces, and elucidate the underlying mechanism of carbon-deposition resistance of Zr/Ni alloy. The preference mechanism of CH_4 formation on both surfaces show that the energetically favorable path1-7 and path1-9 are mainly responsible for Ni(211) with the overall activation energy of 2.22 and 2.24 eV, respectively. Meanwhile, path 2–5 is the most favorable with the overall activation energy of 1.59 eV on ZrNi(211). As compared to Ni(111), the activity of CH_4 formation follows the order: ZrNi(211) > Ni(211) > Ni(111). On the other hand, on Ni(111), CH_4 formation is kinetically competitive with CH_3OH formation. However, Ni(211) can promote CH_4 production and suppress CH_3OH formation simultaneously. More importantly, ZrNi(211) can even maximize the desirable product of CH_4, and lead to no CH_3OH yield. Comparatively, the selectivity of CH_4 follows the order: ZrNi(211) > Ni(211) > Ni(111).

The reason that carbon deposition is unlikely to occur on Ni(111) is that CH preferred to be hydrogenated to CH_2 rather than being dissociated into C. However, Ni(211) is much susceptible to deactivation by coke, this ascribes to the competition of CH_2 between hydrogenation and dehydrogenation as well as the dissociation of COH. Interesting, ZrNi(211) exhibits high resistance of coke deposition because CH_2 hydrogenation is superior to CH_2 dissociation.

Conclusively, Ni(211) shows a significant increase of the selectivity toward CH_4 compared to Ni(111), further, ZrNi(211) displays a remarkable increase in reactivity of CH_4 formation as well as carbon-deposition resistance. In fact, the geometries are very similar, the main difference is the step Zr, which have the higher d-states and the stronger interaction with HCO, CH_2OH and CH_3OH, this agrees with the role of Zr for CH_4 formation.

Acknowledgment

Appendix A. Supplementary data

The descriptions about all possible elementary reactions involving in CH_4, H_2O and CH_3OH formations on Ni(211) and ZrNi(211) surfaces, Microkinetic modeling, and the movies for the most favorable pathways of CH_4 formations on Ni(211) and ZrNi(211) surfaces have been presented in detail. Supplementary data associated with this article can be found, in the online version, at http://dx.doi.org/10.1016/j.mcat.2017.05.012.

References

[1] C.L. Guo, Y.Y. Wu, H.Y. Qin, J.L. Zhang, Fuel Process Technol. 124 (2014) 61–69.
[2] J.F. Zhang, Y.X. Bai, Q.D. Zhang, X.X. Wang, T. Zhang, Y.S. Tan, Y.Z. Han, Fuel 132 (2014) 211–218.
[3] Y. Zeng, H.F. Ma, H.T. Zhang, W.Y. Ying, D.Y. Fang, Fuel 137 (2014) 155–163.
[4] H.L. Lu, X.Z. Yang, G.J. Gao, K.B. Wang, Q.Q. Shi, J. Wang, C.H. Han, J. Liu, M. Tong, X.Y. Liang, C.F. Li, Int. J. Hydrogen Energy 39 (2014) 18894–18907.
[5] F.H. Meng, Z. Li, F.K. Ji, M.H. Li, Int. J. Hydrogen Energy 40 (2015) 8833–8843.
[6] D.W. Goodman, R.D. Kelley, T.E. Madey, J.T. Yates Jr., J. Catal. 63 (1980) 226–234.
[7] B. Miao, S.S.K. Ma, X. Wang, H.B. Su, S.H. Chan, Catal. Sci. Technol. 6 (2016) 4048–4058.
[8] M.P. Andersson, F. Abild-Pedersen, I.N. Remediakis, T. Bligaard, G. Jones, J. Engbæk, O. Lytken, S. Horch, J.H. Nielsen, J. Sehested, J.R. Rostrup-Nielsen, J.K. Nørskov, I. Chorkendorff, J. Catal. 255 (2008) 6–19.
[9] R.Z.C. van Meerten, J.G. Vollenbroek, M.H.J.M. de Croon, P.F.M.T. van Nisselrooy, J.W.E. Coenen, Appl. Catal. 3 (1982) 29–56.
[10] J. Klose, M. Baerns, J. Catal. 85 (1984) 105–106.
[11] R.C. Catapan, A.A.M. Oliveira, Y. Chen, D.G. Vlachos, J. Phys. Chem. C 116 (2012) 20281–20291.
[12] C.M. Zhi, Q. Wang, B.J. Wang, D.B. Li, R.G. Zhang, RSC Adv. 5 (2015) 2873–2877.
[13] J. Engbæk, O. Lytken, J.H. Nielsen, I. Chorkendorff, Surf. Sci. 602 (2008) 733–743.
[14] Y.X. Wang, Y. Su, M.Y. Zhu, L.H. Kang, Int. J. Hydrogen Energy 40 (2015) 8864–8876.
[15] Q. Liu, F.N. Gu, J.J. Gao, H.F. Li, G.W. Xu, F.B. Su, J. Energy Chem. 23 (2014) 761–770.
[16] A.H. Chen, T. Miyao, K. Higashiyama, M. Watanabe, Catal. Sci. Technol. 4 (2014) 2508–2511.
[17] N. Perkas, G. Amirian, Z.Y. Zhong, J. Teo, Y. Gofer, A. Gedanken, Catal. Lett. 130 (2009) 455–462.
[18] X.P. Lu, F.N. Gu, Q. Liu, J.J. Gao, Y.J. Liu, H.F. Li, L.H. Jia, G.W. Xu, Z.Y. Zhong, F.B. Su, Fuel Process Technol. 135 (2015) 34–46.
[19] J. Barrientos, M. Lualdi, R.S. París, V. Montes, M. Boutonnet, S. Järås, Appl. Catal. A 502 (2015) 276–286.
[20] J.L.C. Fajín, J.R.B. Gomes, M.N.D.S. Cordeiro, J. Phys. Chem. C 119 (2015) 16537–16551.
[21] S.V. Eremeev, L.Y. Nemirovich-Danchenko, S.E. Kul'Kova, Phys. Solid State 50 (2008) 543–552.
[22] O.I. Malyi, V.V. Kulish, K. Bai, P. Wu, Z. Chen, Surf. Sci. 611 (2013) 5–9.
[23] Y. Xu, C. Fan, Y.A. Zhu, P. Li, X.G. Zhou, D. Chen, W.K. Yuan, Catal. Today 186 (2012) 54–62.
[24] R.A. Van Santen, M. Neurock, S.G. Shetty, Chem. Rev. 110 (2010) 2005–2048.
[25] G.A. Somorjai, Wiley, New York, 1994.
[26] T. Zambelli, J. Wintterlin, J. Trost, G. Ertl, Science 273 (1996) 1688–1690.
[27] G. Kresse, J. Furthmüller, Phys. Rev. B 54 (1996) 11169–11186.
[28] G. Kresse, J. Hafner, Phys. Rev. B 48 (1993) 558–561.
[29] G. Kresse, D. Joubert, Phys. Rev. B 59 (1999) 1758–1775.
[30] S. Grimme, J. Comp. Chem. 27 (2006) 1787–1799.
[31] J.P. Perdew, J.A. Chevary, S.H. Vosko, K.A. Jackson, M.R. Pederson, D.J. Singh, C. Fiolhais, Phys. Rev. B 46 (1993) 6671–6687.
[32] M. Methfessel, A.T. Paxton, Phys. Rev. B 40 (1989) 3616–3621.
[33] H.J. Monkhorst, J.D. Pack, Phys. Rev. B 13 (1976) 5188–5192.
[34] A.H. Zhang, J. Zhu, W.H. Duan, Surf. Sci. 601 (2007) 475–478.
[35] D. Sheppard, P. Xiao, W. Chemelewski, D.D. Johnson, G. Henkelman, J. Chem. Phys. 136 (2012) 385–404.
[36] D. Sheppard, R. Terrell, G. Henkelman, J. Chem. Phys. 128 (2008) 134106–134110.
[37] J. Wellendorff, T.L. Silbaugh, D. Garcia-Pintos, J.K. Nørskov, T. Bligaard, F. Studt, C.T. Campbell, Surf. Sci. 640 (2015) 36–44.
[38] N. Kapur, J. Hyun, B. Shan, J.B. Nicholas, K. Cho, J. Phys. Chem. C 114 (2010) 10171–10182.
[39] R.G. Zhang, X.Q. Guo, B.J. Wang, L.X. Ling, J. Phys. Chem. C 119 (2015) 14135–14144.
[40] F.L. Che, A.J. Hensley, S. Ha, J.-S. McEwen, Catal. Sci. Technol. 4 (2014) 4020–4035.
[41] T. Mori, A. Miyamoto, N. Takahashi, M. Fukagaya, H. Niizuma, T. Hattori, Y. Murakami, J. Chem. Soc. Chem. Commun. 11 (1984) 678–679.
[42] T. Mori, A. Miyamoto, N. Takahashi, M. Fukagaya, T. Hattori, Y. Murakami, J. Phys. Chem. 90 (1986) 5197–5201.
[43] W.M.H. Sachtler, D.F. Shriver, W.B. Hollenberg, A.F. Lang, J. Catal. 92 (1985) 429–431.
[44] R.G. Zhang, F. Liu, B.J. Wang, Catal. Sci. Technol. 6 (2016) 8036–8054.
[45] Z.J. Zuo, F. Peng, W. Huang, Sci. Rep. 6 (2016) 34670.
[46] Z.X. Chen, H.A. Aleksandrov, D. Basaran, N. Rösch, J. Phys. Chem. C 114 (2010) 17683–17692.
[47] Z.J. Zhao, C.C. Chiu, J.L. Gong, Chem. Sci. 6 (2015) 4403–4425.
[48] J. Sehested, S. Dahl, J. Jacobsen, J.R. Rostrup-Nielsen, J. Phys. Chem. B 109 (2005) 2432–2438.
[49] J.J. Gao, Q. Liu, F.N. Gu, B. Liu, Z.Y. Zhong, F.B. Su, RSC Adv. 5 (2015) 22759–22776.
[50] J.D. Li, E. Croiset, L. Ricardez-Sandoval, J. Phys. Chem. C 117 (2013) 16907–16920.
[51] X.H. Yu, S.G. Wang, Y.W. Li, J.G. Wang, H.J. Jiao, J. Phys. Chem. C 116 (2012) 10632–10638.
[52] A.R. Puigdollers, S. Tosoni, G. Pacchioni, J. Phys. Chem. C 120 (2016) 15329–15337.